Antenna Arrays as Millimeter-Wave Wireless Interconnects in Multichip Systems

Rounak Singh Narde , *Student Member, IEEE*, Jayanti Venkataraman , *Senior Member, IEEE*, Amlan Ganguly , *Member, IEEE*, and Ivan Puchades , *Member, IEEE*

Abstract—In this letter, the transmission characteristics between on-chip arrays and their beamforming capabilities for intrachip and interchip communication in multichip systems are simulated and measured using various fabricated arrays on silicon chips. The measured intrachip and interchip maximum transmission coefficients for various arrays without metal sheets range from −37 to −45 dB and −46 to −51 dB, respectively at 60 GHz. The beamforming for arrays with and without feed structures is compared by radiation pattern using simulations. Moreover, the transmission with metal sheets, emulating realistic multicores, shows a reduction of about 10 dB for intrachip communication compared with cases having no sheets. In this letter, we have demonstrated that beamforming and beam steering can be successfully achieved.

Index Terms—Inter- and intrachip transmission, millimeter-wave (mmWave) interconnect, multichip system, network-on-chip.

I. INTRODUCTION

IN THIS age of information, the explosion of advanced technologies like virtual reality, Internet of Things (IoT), cloud computing, etc., has created enormous pressure on data processing in datacenters. One of the major challenges is to improve data transfer using traditional metal interconnects connecting multiple cores in a high-performance multichip multicore (MCMC) computing system. Much research has shown that wireless interconnects (WIs), which are implemented using on-chip antennas, operating in millimeter-wave (mmWave) bands can reduce energy consumption and increase the bandwidth of chip-to-chip communication drastically as compared to the metallic interconnect based MCMC systems [1]–[4]. Recently in [5], we published a study of transmission coefficients between WIs implemented as zigzag antennas placed at different locations across the chip for intrachip and interchip communications in an MCMC system.

In this letter, a four-element linear phased array antenna system is implemented as WI operating at 60 GHz frequency to study on-chip beamforming. The motivation to study beamforming is to eventually enable beam-steering. Beam-steering using phased arrays will be helpful to direct the radiation toward desired WI, therefore enabling spectral reuse and eventually higher
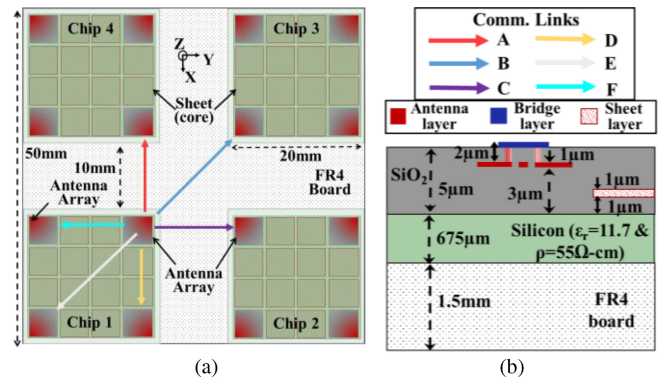
Fig. 1. (a) Top view of a MCMC system showing various communication links between wireless nodes influenced from [5]. (b) Side view of the multichip-multicore system. (not to scale)

data rates for intrachip and interchip wireless communications. In Fig. 1, a simplified arrangement of four chip MCMC system is shown with its side view, which is influenced by [5]. Each corner of the chip has a WI that is shown in red color. This WI requires wireless links in fixed directions at a time. Link A, B, and C connect WIs between different chips–interchip links, and link D, E, and F connect WI within the same chip–intrachip links. In this way, the antenna radiation can be directed toward the desired direction. Since the required beam directions are fixed, multiple directional antennas may be used, but it will increase the area overhead on the chip. However, a phased array uses the same antenna elements to steer the beam, but a compact feed system is required.

Contributions of this letter are as follows.
1) Design and fabrication of on-chip array with feed system.
2) Demonstration of beamforming using radiation pattern.
3) Measurement of transmission coefficients between on-chip arrays for intrachip and interchip communications.

In [6], Abadal *et al*. have stressed beamforming for wireless network-on-chip using simulation-based work. In the literature, most of the work-related mmWave arrays and beamforming are performed for 5G and 60 GHz WiGig systems which are fabricated on substrates other than silicon [7]–[10]. Few works by Babakhani *et al*. [11] and Sengupta *et al*. [12] have shown the implementation of silicon-based mmWave arrays with applications to off-chip communication and THz imaging.

Zigzag antenna, shown in Fig. 2 and used in [2] and [5], is preferred as an element because of its compact size and sufficiently omnidirectional pattern on a silicon chip. Moreover, Table I shows that the radiation efficiency of the zigzag antenna compared reasonably well with other recent works related to on-chip antennas. In this letter, our primary goal is to demonstrate
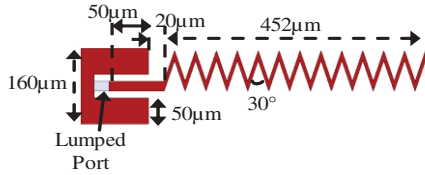
Fig. 2.   Zigzag antenna element.

TABLE I
COMPARISON OF RADIATION EFFICIENCIES OF ON-CHIP ANTENNAS

Ref.	Year	Antenna	Radiation Efficiency
[16]	2017	dipole w/ AMC	22.7% (at 94GHz)
[17]	2018	Vivaldi (CMOS)	20% (at 60GHz)
[5]	2020	Zigzag (CMOS)	15% (at 60GHz)

beamforming and beam steering. To be able to experimentally validate this concept, we have used a passive feed system with path length variations for phasing the antenna elements. Various techniques typically used to implement beam-steering electronically are noted in [13]–[15]. Following is the discussion on simulation and measurement of the on-chip arrays.

II. SIMULATION AND EXPERIMENTAL RESULTS

In this section, the design, simulation, and measurement of the four-element phased array system are discussed. As shown in Fig. 1(a), six links are desired. The angle between link A, B, and C is 45°, and same between links D, E, and F. So, the links B and E can be designed as broadside array, and others can be designed as phased arrays with beam max in direction of 45° from the direction of link B and E. As the antenna element in consideration is a zigzag antenna, therefore, to cover all the link directions, the elements are arranged 45° to the sides of the chip. Moreover, when the four-elements are arranged with a spacing of $3\lambda/8$ (≈ 0.75 mm) in the way shown in Fig. 3(a), the total radiation of array in its axial direction is expected to have a null. Therefore, additional orientation of antenna is selected where the elements are placed orthogonal to the array axis as shown in Fig. 3(b) for endfire radiation. Hence, two different antenna orientations are considered: axial (A) and orthogonal (O).

In Fig. 1(b), the side view of the MCMC system is shown. The silicon chips ($\varepsilon_r = 11.7$ and $\rho = 55 \ \Omega$cm) of thickness 675 μm are placed on 1.5 mm thick FR4 ($\varepsilon r = 4.4$ and $\tan(\delta) = 0.02$) board. The aluminum antenna arrays are placed in antenna layer which is at the height of 3 μm from silicon. The arrangement is simulated in ANSYS HFSS. The simulations are performed with individual lumped ports having progressive phase variation as 0°, 96°, and 135° for broadside ($\phi_m = 90°$), phased ($\phi_m = 45°$) and endfire ($\phi_m = 180°$) arrays. The progressive phase is calculated by theoretical equations for four-elements with a spacing of $3\lambda/8$ (≈ 0.75 mm). These HFSS simulations are performed to ensure that the array is forming proper beams. From the S_{11} plots in Fig. 3(c) and (d), it can be seen that the antenna elements are resonating at 60 GHz with a magnitude of about -30 dB. Mutual coupling between elements is shown in Fig. 3(e) and (f).

The next simulations are performed with coplanar waveguide (CPW) feed structures along with the ground-signal-ground (GSG) pads required for measurement. The complete array structures are shown in Fig. 4. To make sure that the CPW feeds operate in proper modes, both side grounds are connected by
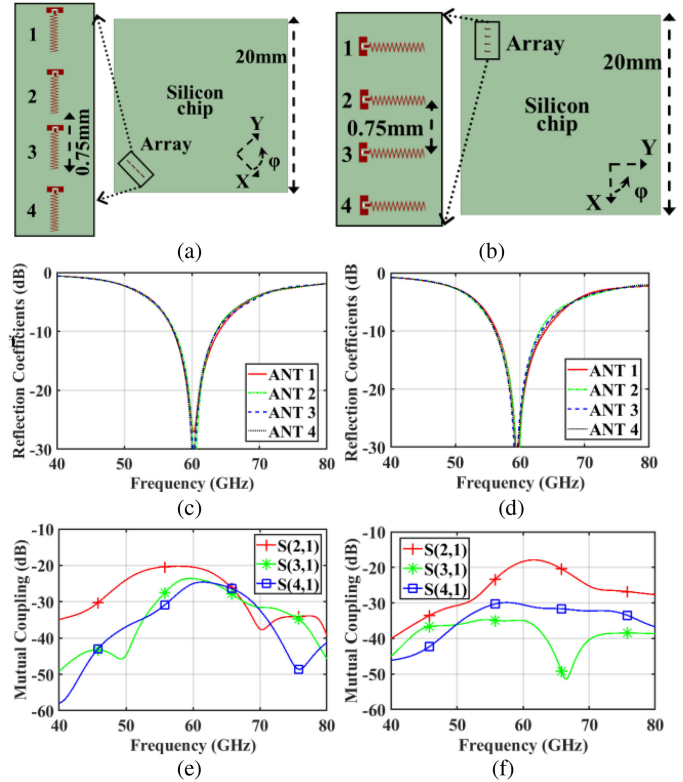

Fig. 3.   Zigzag antenna arrangement without feed, but HFSS ports on silicon chip: (a) axial; (b) orthogonal. Reflection coefficients: (c) axial; (d) orthogonal. Mutual couplings: (e) axial; (f) orthogonal.

metal bridges. These bridges are designed in aluminum layer 1 μm above the antenna layer as shown in Fig. 1(b).

The antenna array system is fabricated using standard CMOS process in Semiconductor and Microsystems Fabrication Laboratory (SMFL) at Rochester Institute of Technology. The arrays on silicon chips are fabricated in various orientations considering the feasible measuring scenarios and movements of probes arms of the probe station. Since the metal wiring in oxide layer over processor core on silicon is modeled by simulations as single metal sheet in oxide layer due to high density of metal wire [5], the metal sheets emulate realistic cores on the chip. Few chips are designed with these sheets as shown in Fig. 1(a) to compare the effect of cores of the chip.

The measurement setup involves Cascade probe station along with GSG probes and Keysight N5247B PNA-X. The probe station is customized with a low-loss dielectric chuck. The PNA-X is calibrated using SOLT (short-open-load-thru) method with Cascade impedance standards substrate. As noted in the previous section that the antenna arrays have probe pads which feed the antennas, these pads act as parasitics. To remove its effect, the calibration reference plane is adjusted in postprocessing steps. Collective simulated and measured results like S_{11}, radiation pattern, and transmission coefficients are shown in Fig. 5. Furthermore, the simulation results for the design with metal sheets are not available, since the computational requirements are too high. Therefore, only measurements of transmission coefficients are shown for various arrays.

The arrangement of the broadside, phased, and endfire arrays for intrachip scenarios is shown in Fig. 5(a)–(c), respectively. From the S_{11} plots shown in Fig. 5(d)–(f), it can be seen that the antenna arrays are working at 60 GHz frequency band with
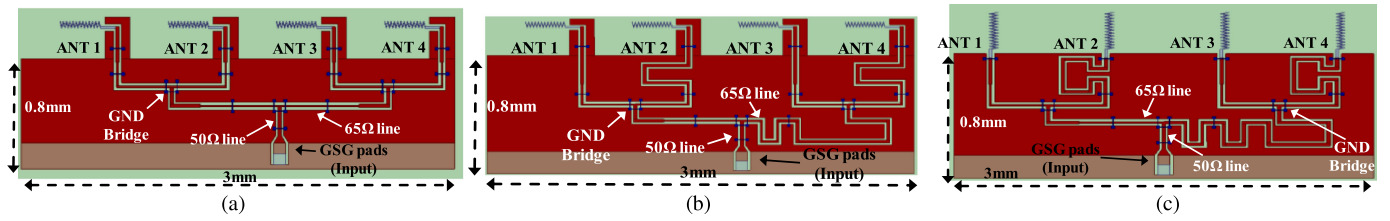
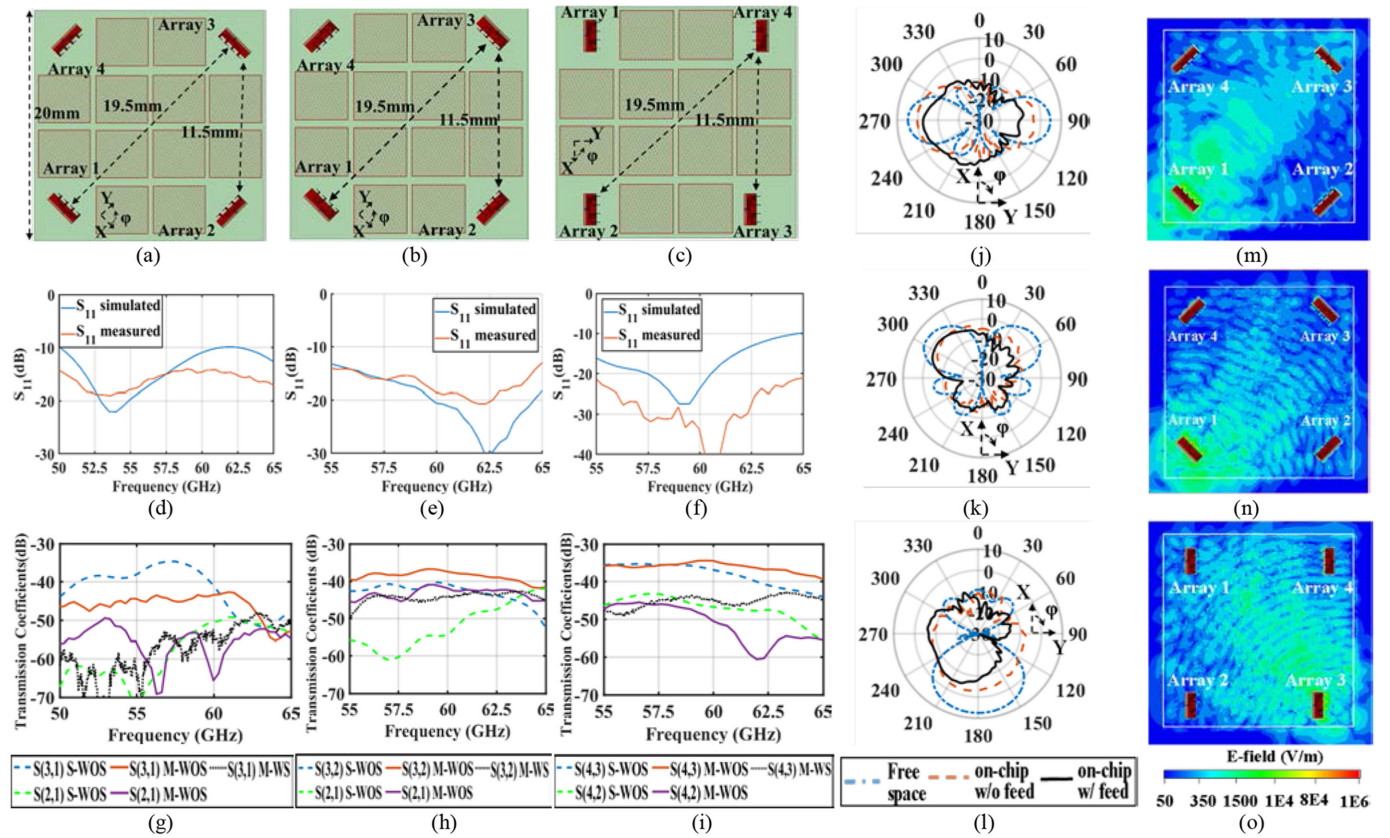Fig. 4.   Array with feed system. (a) Broadside. (b) Phased. (c) Endfire.

Fig. 5.   Intrachip array arrangement for (a) broadside, (b) phased, and (c) endfire. Simulated and measured S_{11} of the array for (d) broadside, (e) phased, and (f) endfire. Simulated and measured transmission coefficients between arrays: (g) broadside, (h) phased, and (i) endfire. Simulated radiation pattern of the array in free space without feed, on silicon with and without feed: (j) broadside–excited array 1 only, (k) phased–excited array 1 only, (l) endfire–excited array 1 only. Simulated electric field distribution across the chip: (m) broadside array–excited array 1 only, (n) phased array–excited array 1 only, (o) endfire array–excited array 3 only. (S-WOS–simulated without metal sheets; M-WOS–measured without metal sheets; M-WS–measured with sheets).

both simulated and measured S_{11} magnitude below −10 dB. In Fig. 5(j)–(l), the comparison between simulated radiation patterns of broadside, phased, and endfire arrays are performed in free space, on-chip without the feed but each antenna element excited by individual HFSS ports, and on-chip array with feed system. The free-space radiation pattern of arrays shows sharp beamforming toward desired directions. Free-space radiation pattern are only provided to compare the beamforming of the arrays with other patterns. When the array is placed on the chip, the gain is reduced because the on-chip antenna has lower efficiency of around 15% due to the losses in silicon substrate. Also, the simulated radiation pattern of broadside array 1 in Fig. 5(j) shows that the array with the feed on the chip is radiating toward +Y-axis and −Y-axis which is the expected broadside direction. However, the gain toward +Y-axis is lower compared to −Y-axis; this is because the array 1 is located at the edge of the lossy silicon chip, so the beam toward +Y-axis

has to encounter more lossy substrate. Moreover, the gain of side lobes has increased due to the sharp corners of the chip that causes diffraction of the beam. Similarly, the distortion of the radiation pattern in the case of phased and endfire arrays in Fig. 5(k) and (l) can be explained. Measurement of radiation pattern for intrachip and interchip transmission in the plane of the array or chip requires a standard antenna to be fabricated on the chip at various orientations. It is challenging to fabricate a standard-gain antenna to perform accurate measurements of the antenna-under-test as its gain and radiation pattern will also get impacted by the structures in the chip. This limits the feasibility of the measurement of the radiation pattern of the antenna-under-test within a chip.

The transmission coefficients between broadside array pairs for intrachip communication are plotted in Fig. 5(g) with metal sheets (WS) and without sheets (WOS). Considering broadside array 1, the beam is directed toward array 3, so the transmission

TABLE II
TRANSMISSION COEFFICIENTS FOR INTRACHIP COMMUNICATION AT 60 GHz

	Broadside	Phased	Endfire
S-WOS S(3,1)/S(3,2)/S(4,3)	-41	-41	-37
M-WOS S(3,1)/S(3,2)/S(4,3)	-43	-37	-35
S-WOS S(2,1)/S(2,1)/S(4,2)	-50	-54	-47
M-WOS S(2,1)/S(2,1)/S(4,2)	-66	-42	-50

S_{31} is expected to be greater than the other pair. The simulated and measured transmission without sheets S_{31} is -41 and -43 dB, respectively at 60 GHz. The other transmission coefficient S_{21} without sheets is about 10 dB lower than S_{31} which is expected. Table II shows that the transmission coefficients between arrays for intrachip communication at the desired frequency that is 60 GHz have satisfactory agreement between the simulated and measured results.

However, there are differences in the results from 55 to 65 GHz frequency band. These differences have been studied in [18] and [19], which described many factors responsible such as fabrication process variation, variation in thickness of the substrate, and variation in dielectric constants [20]. So multiple iterations of fabrication are needed to match the simulation to the measurement. Another factor for the difference is the type of calibration technique used for measurement that is SOLT. In [21], authors have found that SOLT introduces some error in the measurement.

When metal sheets, which as shown in [5] emulate the lower levels of metal wires in a multicore chip, are introduced between broadside arrays, then the measured S_{31} reduces about 12 dB. This reduction can be attributed to the destructive interference caused by reflection and diffraction of the radiation due to the metal sheets. The analysis in [5] also showed that the antenna radiation efficiency reduces when metal sheets are used. Finally, the simulated electric field distribution when array 1 is excited without sheets is shown in Fig. 5(m).

The transmission coefficients are plotted for phased arrays for intrachip communication in Fig. 5(h). Due to the feed system arrangement, the array 2 and array 3 have beam focused toward each other. So, the transmission between array 2 and 3 is expected to be maximum. The measured and simulated transmission coefficients are shown in Table II. The electric field distribution is shown in Fig. 5(n). Similarly, for endfire arrays in Fig. 5(c), the arrays 3 and 4 have beams directed toward each other, so this pair is expected to have highest transmission. The simulated and measured S_{43} without sheet (WOS) are -37 and -35 dB, respectively. This is more than 10 dB higher than the measured transmission for the other pair S_{42}. The transmission reduced to -44 dB (WS) compared to WOS case. The electric field distribution is shown in Fig. 5(o).

Finally, the results of simulated and measured interchip transmission scenarios are shown in Fig. 6. The zoomed-in top-views of all three types of array arrangement in interchip scenario are shown in Fig. 6(a)–(c). Since, these are the same arrays from intrachip scenario so the reflection coefficients are same, which are shown in Fig. 5. For broadside arrays WOS, the interchip simulated and measured transmission, shown in Fig. 6(d), between array 1 and array 3 is -36 and -46 dB, respectively, at 60 GHz. This is much higher than S_{21} at 60 GHz for simulated and measured cases. In case of phased array, due to the phase variation provided by the feed, arrays 1 and 2, shown in Fig. 6(b), have beams directed at each other. In Fig. 6(e), the
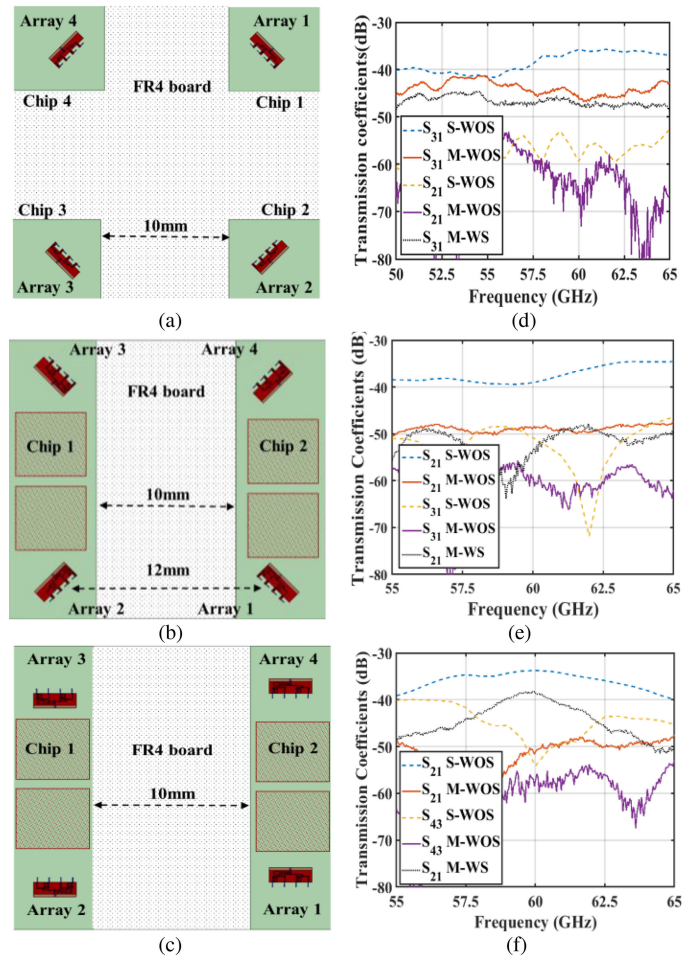

Fig. 6. Interchip arrangement of arrays: (a) broadside, (b) phased, and (c) endfire. Simulated and measured transmission coefficients between arrays (d) broadside, (e) phased, and (f) endfire. (S-WOS–simulated without metal sheets; M-WOS–measured without metal sheets; M-WS–measured with sheets).

interchip simulated and measured transmission S_{21} are -39 and -48 dB, respectively at 60 GHz. For the case of endfire array as arranged in Fig. 6(c), the maximum transmission without sheets is between array 1 and array 2 which is -34 dB (simulated) and -51 dB (measured). The differences between simulated and measured results are due to the environment not being exactly the same because of the metal parts of the probe station. Overall, we can observe that the metal sheets do not affect the interchip transmission.

III. CONCLUSION

In this letter we have demonstrated that beam steering can be successfully achieved in specified directions. Therefore, we can conclude that beam steering can be achieved in multiple directions with these arrays when they are phased electronically. This letter also presents transmission between on-chip arrays for intrachip and interchip communication in MCMC systems. The measured intrachip and interchip highest-achieved transmission coefficients for various arrays without metal sheets range from -37 to -45 dB and -46 to -51 dB, respectively, at 60 GHz. Moreover, the metal sheets, emulating realistic multicores, have reduced transmission coefficients for intrachip communication by about 10 dB compared with cases having no sheets. This will be helpful when designing link budget for an on-chip wireless system.

REFERENCES

[1] A. Ganguly, K. Chang, S. Deb, P. P. Pande, B. Belzer, and C. Teuscher, "Scalable hybrid wireless network-on-chip architectures for multicore systems," *IEEE Trans. Comput.*, vol. 60, no. 10, pp. 1485–1502, Oct. 2011.

[2] M. S. Shamim, N. Mansoor, R. S. Narde, V. Kothandapani, A. Ganguly, and J. Venkataraman, "A wireless interconnection framework for seamless inter and intra-chip communication in multichip systems," *IEEE Trans. Comput.*, vol. 66, no. 3, pp. 389–402, Mar. 2017.

[3] S. Laha, S. Kaya, D. W. Matolak, W. Rayess, D. DiTomaso, and A. Kodi, "A new frontier in ultralow power wireless links: Network-on-chip and chip-to-chip interconnects," *IEEE Trans. Comput.-Aided Des. Integr. Circuits Syst.*, vol. 34, no. 2, pp. 186–198, Feb. 2015.

[4] S. Abadal *et al.*, "Scalability of broadcast performance in wireless network-on-chip," *IEEE Trans. Parallel Distrib. Syst.*, vol. 27, no. 12, pp. 3631–3645, Dec. 2016.

[5] R. S. Narde, J. Venkataraman, A. Ganguly, and I. Puchades, "Intra- and inter-chip transmission of millimeter-wave interconnects in NoC-based multi-chip systems," *IEEE Access*, vol. 7, pp. 112200–112215, 2019.

[6] S. Abadal *et al.*, "Opportunistic beamforming in wireless network-on-chip," in *Proc. IEEE Int. Symp. Circuits Syst.*, Sapporo, Japan, 2019, pp. 1–5.

[7] Y. Huo, X. Dong, W. Xu, and M. Yuen, "Enabling multi-functional 5G and beyond user equipment: A survey and tutorial," *IEEE Access*, vol. 7, pp. 116975–117008, 2019.

[8] I. A. Hemadeh, K. Satyanarayana, M. El-Hajjar, and L. Hanzo, "Millimeter-wave communications: Physical channel models, design considerations, antenna constructions, and link-budget," *IEEE Commun. Surveys Tuts.*, vol. 20, no. 2, pp. 870–913, Apr.–Jun. 2018.

[9] W. Hong, "Solving the 5G mobile antenna puzzle: Assessing future directions for the 5G mobile antenna paradigm shift," *IEEE Microw. Mag.*, vol. 18, no. 7, pp. 86–102, Nov./Dec. 2017.

[10] A. Rashidian, S. Jafarlou, A. Tomkins, K. Law, M. Tazlauanu, and K. Hayashi, "Compact 60 GHz phased-array antennas with enhanced radiation properties in flip-chip BGA packages," *IEEE Trans. Antennas Propag.*, vol. 67, no. 3, pp. 1605–1619, Mar. 2019.

[11] A. Babakhani, X. Guan, A. Komijani, A. Natarajan, and A. Hajimiri, "A 77 GHz phased-array transceiver with on-chip antennas in silicon: Receiver and antennas," *IEEE J. Solid-State Circuits*, vol. 41, no. 12, pp. 2795–2806, Dec. 2006.

[12] K. Sengupta and A. Hajimiri, "A 0.28 THz power-generation and beam-steering array in CMOS based on distributed active radiators," *IEEE J. Solid-State Circuits*, vol. 47, no. 12, pp. 3013–3031, Dec. 2012.

[13] S. Ghosh and D. Sen, "An inclusive survey on array antenna design for millimeter-wave communications," *IEEE Access*, vol. 7, pp. 83137–83161, 2019.

[14] A. Chakraborty and B. Gupta, "Paradigm phase shift: RF MEMS phase shifters: An overview," *IEEE Microw. Mag.*, vol. 18, no. 1, pp. 22–41, Jan./Feb. 2017.

[15] S. Shamsadini, I. M. Filanovsky, P. Mousavi, and K. Moez, "A 60 GHz transmission line phase shifter using varactors and tunable inductors in 65 nm CMOS technology," *IEEE Trans. Very Large Scale Integration Syst.*, vol. 26, no. 10, pp. 2073–2084, Oct. 2018.

[16] M. Nafe, A. Syed, and A. Shamim, "Gain-enhanced on-chip folded dipole antenna utilizing artificial magnetic conductor at 94 GHz," *IEEE Antennas Wireless Propag. Lett.*, vol. 16, pp. 2844–2847, 2017.

[17] K. S. Sultan, H. H. Abdullah, E. A. Abdallah, M. A. Basha, and H. H. El-Hennawy, "A 60-GHz gain enhanced vivaldi antenna on-chip," in *Proc. IEEE Int. Symp. Antennas Propag.*, 2018, pp. 1821–1822.

[18] H. Zhang and A. Shamim, "Tackling the issues of millimeter-wave on-chip antenna measurements," *Proc. 13th Eur. Conf. Antennas Propag.*, Krakow, Poland, 2019, pp. 1–5.

[19] A. C. F. Reniers, Q. Liu, M. H. A. J. Herben, and A. B. Smolders, "Review of the accuracy and precision of mm-wave antenna simulations and measurements," in *Proc. 10th Eur. Conf. Antennas Propag.*, 2016, pp. 1–5.

[20] A. Papio Toda and F. De Flaviis, "60 GHz substrate materials characterization using the covered transmission-line method," *IEEE Trans. Microw. Theory Techn.*, vol. 63, no. 3, pp. 1063–1075, Mar. 2015.

[21] Q. Li and K. L. Melde, "The impact of on-wafer calibration method on the measured results of coplanar waveguide circuits," *IEEE Trans. Adv. Packag.*, vol. 33, no. 1, pp. 285–292, Feb. 2010.